Steady/Unsteady RANS Simulations of Heat Transfer on a Turbine Vane Endwall with Inlet Boundary Layer Skew

*Xing Yang, Zhenping Feng**

Shaanxi Engineering Laboratory of Turbomachinery and Power Equipment,
Institute of Turbomachinery, School of Energy and Power Engineering,
Xi'an Jiaotong University, Xi'an, Shaanxi 710049, China
*E-mail: zpfeng@mail.xjtu.edu.cn

Terrence W. Simon

Department of Mechanical Engineering,
University of Minnesota, Minneapolis, MN 55455, USA

ABSTRACT

In this study, steady Reynolds-averaged Navier-Stokes (RANS) and unsteady RANS (URANS) simulations in a turbine vane cascade are performed to study the effects of inlet boundary layer skew on flowfields in the vane passage and heat transfer over the endwall surfaces. The inlet skew simulates the relative movement between rotor platform and stator endwall in a turbine stage. The transverse motion of a moving wall, which is placed parallel to and upstream of the vane endwall, generates the inlet skew. An engine-like velocity profile yields a cascade inlet Reynolds number of 3.46×10^5. A parametric study is conducted for two moving wall-to-freestream velocity ratios (r) of 0.61 and 0.76, representing the actual operation of an engine. In addition, steady and time-averaged results are compared to address the difference of predictions in heat transfer from the steady and unsteady simulations. The results show that the effects of unsteadiness due to inherent unsteadiness in the flow and inlet skew passage on the pressures over the endwall surface is negligible. However, the unsteadiness plays an important role in determining endwall heat transfer patterns. The inlet boundary layer skew modifies the development and migration of horseshoe vortex and passage vortex, resulting in local variation of heat transfer over most endwall surfaces. Lower heat transfer coefficients are found near the suction side beyond the passage throat, but overall heat transfer levels almost remain the same on the endwall in the presence of inlet skew.

KEYWORDS

Gas Turbine Endwall, Heat Transfer, Inlet Boundary Layer Skew, Unsteady Simulations

NOMENCLATURE

C	true chord of vane (mm)	x, y, z	Cartesian coordinates
C_{ax}	axial chord of vane (mm)	y^+	non-dimensional wall distance
h	adiabatic heat transfer coefficient	Δt	time step (s)
Ma	Mach number	α	flow angle (°)
P	vane pitch distance (mm)	Λ	turbulence integral length (mm)
p	pressure (Pa)	ω_x	streamwise vorticity (s^{-1})
Pr	non-dimensional pressure ratio ($p/p_{t,in}$)	**Subscripts**	
q	heat flux (W/m^2)	aw	adiabatic wall
r	wall-to-axial velocity ratio (u_w/u_{in})	ex	outlet
Re	averaged Reynolds number	in	inlet

S	span height (mm)	t	total
T	inlet temperature (K) time period for a full flow cycle (s)	max	maximum
Tu	turbulence intensity (%)	w	y-direction, wall
u	velocity (m/s) x-axis velocity component (m/s)	**Overbars**	
U	velocity magnitude (m/s)	–	laterally-averaged
v	y-axis velocity component (m/s)	=	area-averaged

INTRODUCTION

Heat transfer over a gas turbine endwall remains a significant interest of concern since gas turbine inlet temperatures are ever increasing and combustor exit temperature profiles continue to be more flat with the goal of improving engine efficiency and reducing emission. This in turn means hotter gas to the gas-side surface of the endwall, nearly as high as the peak temperatures at the midspan. More particularly, the endwall experiences strong, three-dimensional and complex secondary flows. The necessity of understanding the endwall heat transfer is, first of all, describing and characterizing endwall nearby flows that dominate typical endwall heat transfer patterns. The generation of secondary flows in a turbine passage is attributed to the cumulative effect of turning of inlet vortices through the blade passages and the presence of the endwall. The flow structures near the endwall mainly features horseshoe vortex and passage vortex. More details of the endwall secondary flows can be found in the work of Wang et al. (1997). Simon and Piggush (2006) made a comprehensive literature survey on secondary flows in turbine passages and highlighted the strong links between the secondary flows and the endwall aerodynamics and heat transfer. Thus, accurate prediction of the detailed distributions of gas-side heat transfer on the turbine endwall is vital to design advanced turbine stages that operate with higher temperatures, reduced coolant usage and improved component lifetime. Studies have been extensively conducted on heat transfer for turbine endwalls. The effects of Reynolds number (Kang et al., 1999), Mach number (Harvey et al., 1999 and Giel et al., 1998), turbulence level (Radomsky and Thole, 2000), boundary layer thickness (Graziani et al., 1980) and surface roughness (Lutum et al., 2015) were well addressed. However, because of the inherent issues associated with moving parts, experimental and numerical heat transfer studies were mostly carried out in a stationary cascade, resulting in results that could not be directly applied to gas turbine design stages because of the neglect of flow interactions between rotors and stators.

A number of studies have demonstrated the impact of upstream passing disturbances on downstream turbine aerodynamics and heat transfer. The interaction of wake passage on subsequent turbine heat transfer was performed by Dullenkopf et al. (1991) using a rotating bar wake generator. Effects of unsteady wake on the vane suction surface boundary layer and heat transfer were found to be strong. Zhang and Han (1995) observed that increasing the passing frequency of the wake inhibited the influence of inlet turbulence on the blade heat transfer. Schobeiri et al. (2005&2007) reported that there was a periodic expansion and contraction of the separation region on the suction surface of a low-pressure turbine blade with the passing of the wake. Regarding the effects on heat transfer over endwall surfaces, the recent measurements by Choi et al. (2017&2018) showed that the upstream passing wakes produced a more uniform distribution in heat transfer.

In addition to cases involving the impacts of upstream disturbances, an oncoming boundary layer skewed by the relative motion between rotor platform and stator endwall was simulated by Carrick (1977) using a moving belt upstream of an impulse turbine cascade. The secondary losses were found to be considerable increase with inlet skew. Bindon (1979&1980) determined that the overall distribution of displacement thickness was not greatly impacted by skewing but the skewing enhanced the crossflow and lifted the passage vortex off the endwall. Later, Walsh and Gregory-Smith (1987) observed that the inlet skew could cause the passage vortex to develop more rapidly. In addition, the pressure-side leg of the horseshoe vortex was found to cross the endwall earlier and the losses generated by the inlet skew were higher than those caused by the inlet boundary layer thickness

(Walsh and Gregory-Smith, 1990). Similarly, Ghosh and Goldstein (2012) found that the inlet skew intensified the generation of the horseshoe vortex and passage vortex and, correspondingly, higher mass transfer coefficients were measured between the midspan of the blade and the endwall.

Computational fluid dynamics (CFD) modeling continues to play an important role in completing the analytical solution of the endwall flows and heat transfer and improving our understanding of critical regions of the turbine passage. There have been numerous computational studies on the topic, a couple of which complement the experimental studies. Pasinato et al. (2004) and Arisi et al. (2016) assessed the abilities of various Reynolds-averaged turbulence models in predicting flow and heat transfer for an endwall of a first-stage vane, showing the Reynolds-averaged Navier-Stokes (RANS) solutions obtained by all the turbulence models were higher than the experimental data in terms of heat transfer coefficients and film cooling effectiveness, particularly in the aft portion of the vane passage. Similar results were found in the work of Papa et al. (2007) and Laveau et al. (2014). Comparisons of solutions from steady and unsteady RANS simulations were made by El-Gabry and Ameri (2011) with upstream passing wakes. The time-averaged solutions showed higher heat transfer levels than the steady values in some regions.

The objectives of the present study are twofold. On the one hand, the unsteady effect of a skewed inlet boundary layer due to relative motion of rotor platform on heat transfer over the subsequent stator endwall is numerically investigated; on the other hand, time-averaged results are compared to steady predictions to examine the difference between unsteady and steady simulations of endwall flow and heat transfer. The inlet boundary layer skew is modeled by a moving wall that is parallel to and upstream of a linear cascade, in which the endwall heat transfer has been experimentally measured in previous literature (Yang et al., 2017). Steady and unsteady simulations of the endwall heat transfer are performed for various wall velocities of 0, 8.94, 17.04 m/s. Comparisons of steady and unsteady results make them appropriate for an improved fundamental understanding of the unsteady flow physics in the vane passage and heat transfer on the endwall, and for assessments of the numerical simulation methods for this work.

COMPUTATIONAL METHODOLOGIES

Steady and unsteady simulations were performed using the commercial code ANSYS CFX 18.0. The steady and time-averaged heat transfer results were compared to relevant experimental data. Structured, hexahedral grids were generated by ANSYS ICEM for the computation domain. A recommended grid convergence index (GCI) method was used to perform the grid-independent test.

Computational Domain and Boundary Conditions

As the flow velocity near the endwall is much lower due to no-slip boundary conditions at the endwall, the flow has a considerable tangential component in the frame of reference of the stator, as indicated in the comparisons of velocity diagrams of free stream and boundary layer over the stator inlet endwall region of Fig. 1. As endwall heat transfer is strongly dependent on the flow near the endwall, it is believed that the skewed approaching boundary layer has significant impacts on the flow within the subsequent stator vane passage and the heat transfer over the endwall. In this study, in order to avoid the introducing of other affecting parameters (e.g. wakes) and to clarify the interaction mechanism of the inlet skew, in isolation, the stage model was reduced into a single stator linear cascade, as shown in Fig. 2. A moving wall parallel to and upstream of the cascade is used to generate the oncoming skewed boundary layer.

The vane investigated in this study was reported in the authors' previous work (Yang et al., 2017), in which heat transfer over the endwall surface was measured. The vane is a high-pressure turbine airfoil, which is characterized by a high flow turning angle of 73 deg. The detailed parameters of the geometry are summarized in Table 1. In order to directly compare predictions with the previous experimental data, the domain inlet was located at $1.33C_{ax}$ upstream of the vane leading edge, where measurements of inlet flow boundary conditions were made, including the parameters of velocity profile (Fig. 3), temperature and total pressure. Measured static pressure was assigned at the domain outlet at $2.8C_{ax}$ downstream of the vane trailing edge. The endwall surface was divided into three

areas (Areas 1, 2 and 3). Adiabatic, non-slip wall boundary condition was applied to Area 1. Area 2 modeled the moving wall, and its leading edge and trailing edge were located at $1.12C_{ax}$ and $0.12C_{ax}$ upstream of the vane leading edge, respectively. The average inlet velocity of the incoming flow was 27.94 m/s, resulting in a cascade passage inlet Reynolds number of 3.46×10^5, based on the true chord length of the vane. The moving wall translated at speeds of 0 (stationary), 8.94 m/s and 17.04 m/s, and yielded wall-to-freestream velocity ratios ($r=u_w/u_{in}$) of 0, 0.32 and 0.61, respectively. This corresponded to typical values of $r \sim O(1)$ in real engine operation conditions. Uniform heat flux was imposed on Area 3 that was the region of interest. Translational periodic boundary conditions were applied to the side surfaces of the domain with the exception of the pressure and suction surfaces of the vane that were no-slip walls.

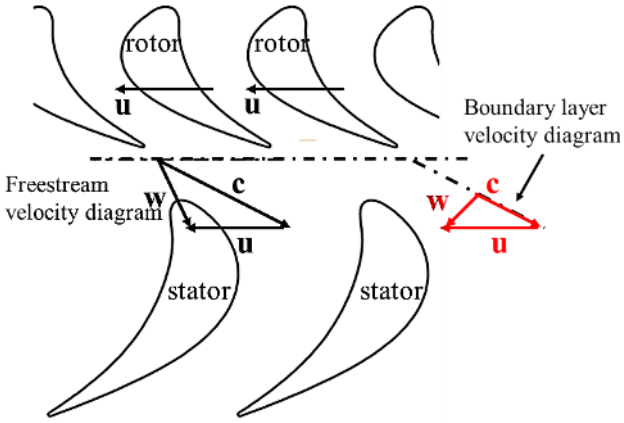

Figure 1: Illustration of boundary layer velocity diagram near endwall

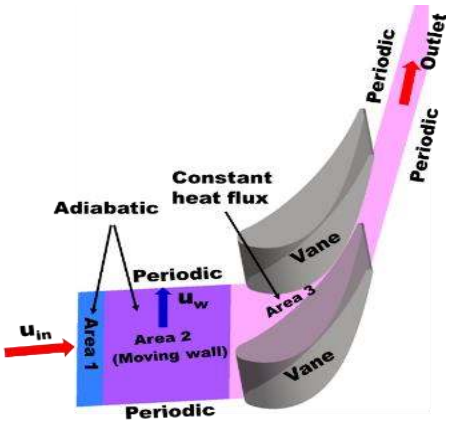

Figure 2: Computational domain and boundary conditions

Table 1: Vane geometry and flow conditions

Parameters	Values	Parameters	Values
True chord length, C/mm	140.30	Inlet flow angle, α_{in}/deg	0
Axial-to-true chord ratio, C_{ax}/C	0.54	Outlet flow angle, α_{ex}/deg	73
Pitch-to-chord ratio, P/C_{ax}	1.42	Inlet Mach Number, Ma_{in}	0.083
Span-to-chord ratio, S/C_{ax}	1.33	Exit Mach Number, Ma_{ex}	0.554
Inlet averaged velocity, u_{in}/m·s^{-1}	27.94	Turbulence intensity, Tu/%	9.8
Inlet temperature, T_{in}/K	293.15	Turbulence integral length, Λ/mm	10
Passage inlet Reynold number, Re_{in}	3.46×10^5	Moving wall speed, u_w/m·s^{-1}	0, 8.94, 17.04

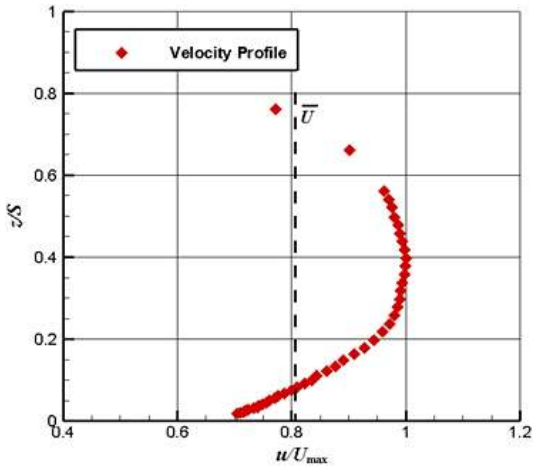

Figure 3: Inlet velocity profile at $1.33C_{ax}$ upstream of the vane leading edge

Numerical Approach

The standard k-ω turbulence model that has been validated by relevant experimental data (Yang et al., 2017) was used to provide closure for the three-dimensional, compressible RANS equations. A default value of 0.85 was retained for the turbulent Prandtl number. High resolution scheme was selected for the spatial discretization. For properties of the air, an ideal gas equation of state was used. Polynomial fits for specific heat capacity vs. temperature and Sutherland's law for thermal conductivity and viscosity were used. The steady solutions were considered to be convergence when the residuals were kept below 10^{-6} and the temperature and flowfield at monitor points remained unchanged. The steady solutions were used to initial the unsteady simulations. In the unsteady simulations, small time-step Δt was set to ensure a sufficient temporal resolution to capture the flow unsteadiness. In this study, for the selected Δt=0.0004 for r=0.32 case and Δt=0.0002 for r=0.61 case, 36 steps were required to complete a cycle, which is a sufficiently fine resolution for this study.

Grid Independency Test

ASNYS ICEM was used to generate structured mesh for the computation domain. Finer grids were applied to the turbine endwall and airfoil surfaces to resolve strong flow and temperature gradients near the walls, resulting in values of y^+ less than 1.0. An established grid convergence index (GCI) method, which is recommended by the Fluids Engineering Division of ASME (Celik et al., 2008), was used to perform grid sensitivity analysis for the RANS simulations. This procedure was fulfilled by using three sequentially refined grids (Table 2) for the calculation of the heat transfer on the endwall. According to the instructions by GCI, the grid refinement was structured evenly in each direction and the refinement factor is greater than 1.3. Table 2 summaries the number of the grid nodes and their area-averaged heat transfer results with deviation from extrapolated values. Figure 4 shows the predicted local heat transfer coefficients along the inviscid streamlines issued from 50% pitch (0.5P) and the solution from the fine grid (grid 3) with discretization errors. The overall difference between the solution from the fine grid and the extrapolated values is 1.53%. The overall discretization uncertainty (GCI values) was 1.29%, far less than 5.0%. Therefore, the fine grid with approximately 4.6 million nodes provided a good accuracy of level and, thus, was used to perform the RANS simulations. Using this grid size, the Courant number in the computation domain is around 1.0 with the exception of a maximum value of 7.0 in a very small area near the vane trailing edge.

Table 2: Area-averaged h from different grids

Grid	Nodes	y^+	$\bar{\bar{h}}$ (W/m²•K)	Deviation of $\bar{\bar{h}}$/%
grid 1	835,270	1.44	225.169	12.12
grid 2	2,141,050	1.02	230.667	9.97
grid 3	4,631,900	0.82	252.310	1.53
extrapolated	—	—	256.224	—

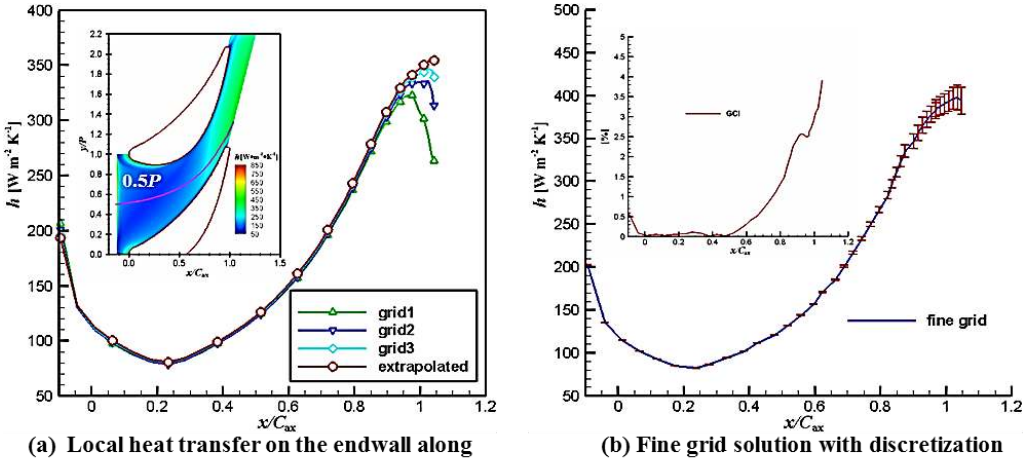

(a) Local heat transfer on the endwall along inviscid streamlines issued at 50% pitch

(b) Fine grid solution with discretization error bars

Figure 4: Grid sensitivity study with GCI method

The heat transfer coefficient in this study is given by

$$h=q/(T_w-T_{aw})$$

where q is specified constant wall heat flux and T_w and T_{aw} are wall temperature and adiabatic wall temperature, respectively. Therefore, in order to calculate heat transfer coefficient defined as such, it is necessary to run two separate analyses; one in which the walls were adiabatic to determine the adiabatic wall temperatures and a second with a prescribed heat flux to calculate the wall temperature.

COMPARISONS OF STEADY AND UNSTEADY RESULTS

In this section, comparisons of the steady and unsteady results are presented with the stationary wall (r=0). The measured data of heat transfer coefficients on the endwall are included as well to validate the reliability of the unsteady simulations. Figure 5 shows the comparison of heat transfer coefficients between measurements (Fig. 5(a)) and predictions from steady (Fig. 5(b)) and unsteady (Fig. 5(c)) simulations. To be more quantitative, heat transfer coefficients are laterally (pitchwise) averaged as functions of axial distance, as shown in Fig. 5 (d). The heat transfer coefficients from the unsteady simulation are time-averaged in a flow cycle. In the fore part of the passage, where the heat transfer level is low, there are slight differences between the steady and time-averaged results, and the steady RANS and URANS predictions agree with the experimental data. However, significant discrepancies are found in the aft portion near and beyond the passage throat. The steady simulations have higher predictions in heat transfer levels than the unsteady simulations. On the basis of the experimental data, the time-averaged results, which takes unsteadiness into consideration, are more reasonable, but the steady RANS over-predicts the heat transfer coefficients because of the neglect of unsteadiness in the flow, as shown in Fig. 5(d).

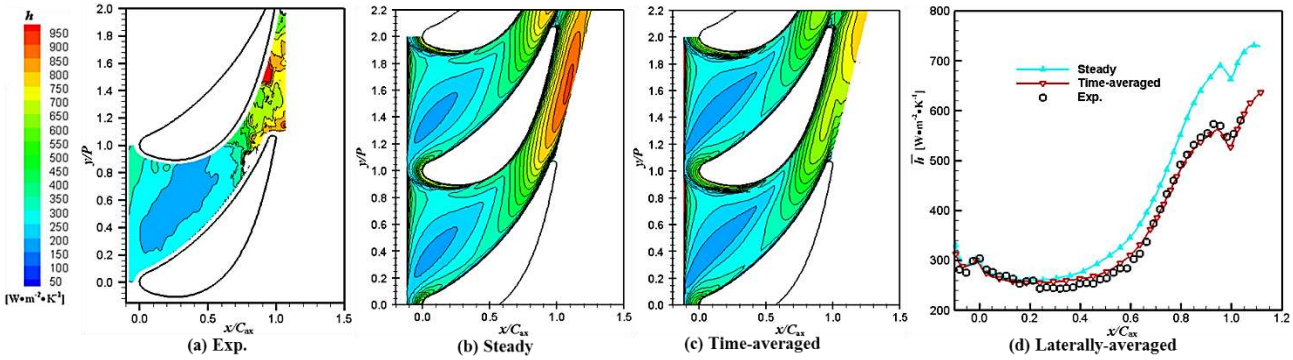

Figure 5: Comparisons of laterally-averaged heat transfer coefficients between measurements (Yang et al., 2017) and steady and time-averaged results

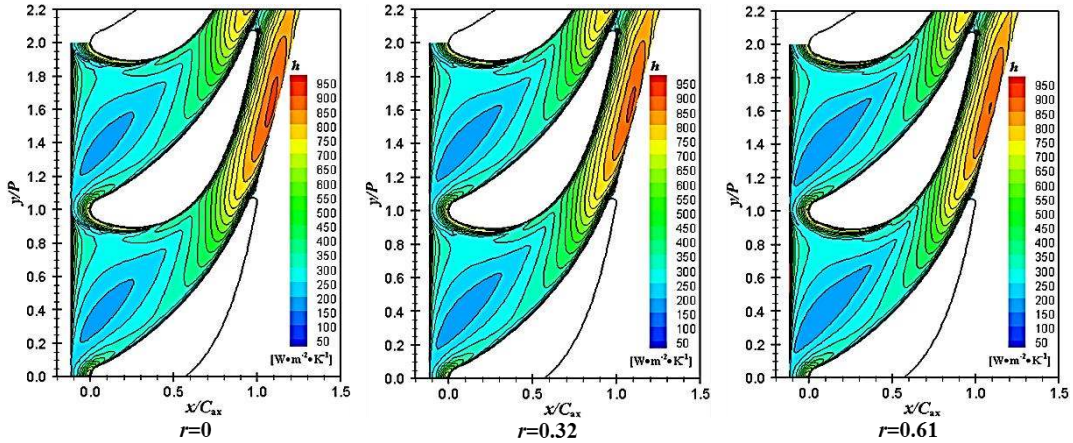

Figure 6: Steady results of heat transfer coefficients on endwall

In order to document the effect of unsteadiness on heat transfer, steady and time-averaged results of heat transfer coefficients with velocity ratios of r=0.32 and r=0.61 are further presented in Figs. 6

and 7, respectively. Slight differences between the steady and time-averaged results are observed upstream of the passage throat. However, beyond the passage throat, the mixing out of various vorticities in the passage and the wake shed from the vane trailing edge add unstable factors into the turbulent flow, resulting in a highly unsteady effect on the endwall heat transfer. This leads to an obvious gap between the steady and time-averaged results. For the steady simulations with an upstream stationary or moving wall, high heat transfer levels are concentrated near the passage exit. Using unsteady simulations, heat transfer appears to be more uniform due to the random unsteadiness. In terms of the values of heat transfer coefficients, the steady results are higher than those from the unsteady simulations regardless of the inlet skewed boundary layer.

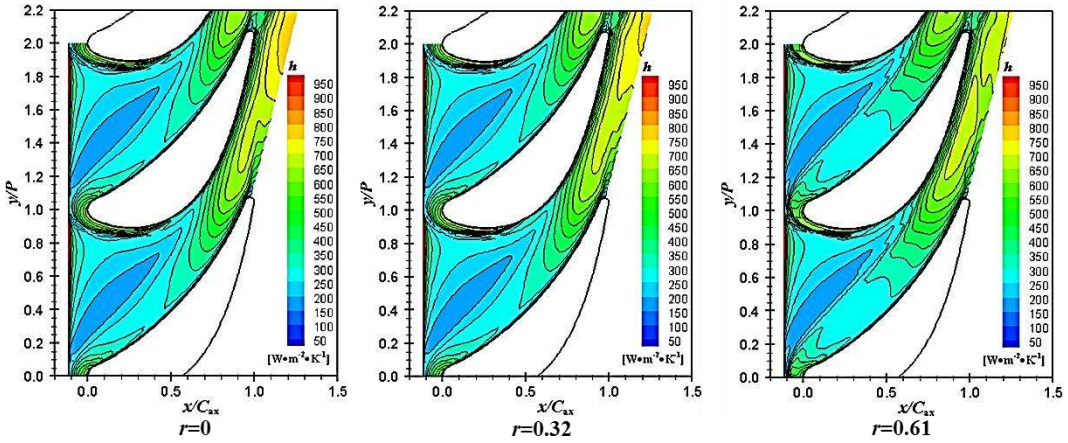

Figure 7: Time-averaged results of heat transfer coefficients on endwall

For a more quantitative comparison of steady RANS and URANS simulations in predicting endwall heat transfer, the differences between steady and time-averaged heat transfer coefficients are displayed in Fig. 8 for the stationary and moving wall cases. The difference is given by ($h_{\text{-steady}}$–$h_{\text{-avg}}$)/ $h_{\text{-avg}}$, where $h_{\text{-steady}}$ and $h_{\text{-avg}}$ are the steady and time-averaged heat transfer coefficients from the steady RANS and URANS simulations, respectively. In comparison with steady results, the time-averaged heat transfer coefficients are about 4%–20% higher in the migration path of the passage vortex from the leading edge of one vane toward the suction side of the companion vane at x/C_{ax}=0.9. This is in accordance with the results obtained by El-Gabry and Ameri (2011). However, the unsteadiness decreases the heat transfer level up to 20% right upstream of the lift-off line of the passage vortex and along the pressure side of the passage all the way beyond the passage exit. Everywhere else, nearly zero difference is presented. Generally, increasing the inlet skew increases the differences in local heat transfer predictions between the steady and time-averaged results with the effect of unsteadiness on the endwall heat transfer being highly localized to the regions affected by the passage vortex and flows with high velocity, indicating the passing effects of the inlet skewed boundary layer.

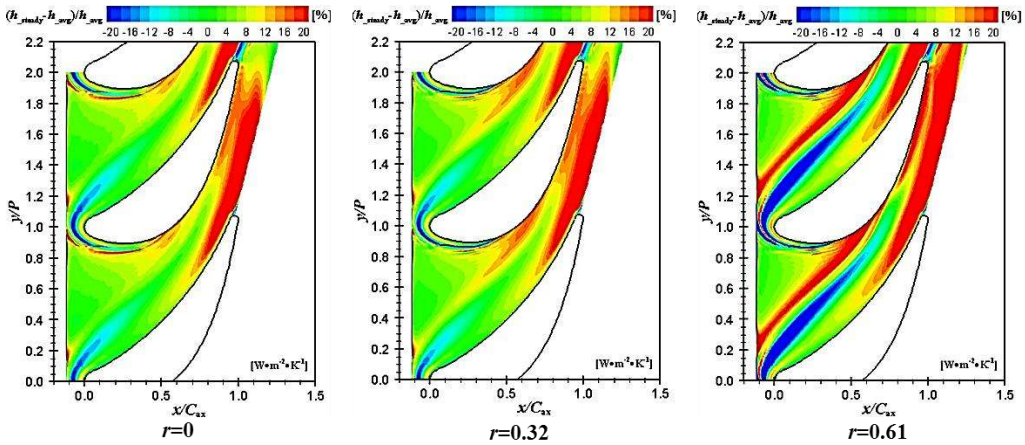

Figure 8: Differences in endwall heat transfer coefficients between the steady and time-averaged results

EFFECTS OF INLET SKEW

The effects of the inlet boundary layer skew on the endwall heat transfer are documented using URANS simulations. Instantaneous pressure distributions, normalized by inlet total pressure, on the endwall surface at equal times over the period of one flow cycle are plotted in Fig. 9, showing the temporal behavior of the flow fields in the passage with and without inlet skewed boundary layers. The non-dimensional time (t/T) values are chosen so that they represent the temporal states within one full period. The local pressure distributions within the passage experience periodic changes. Moderate changes appear upstream of the passage throat and pronounced changes are found in the low pressure region near the suction side beyond the passage throat. The position and extent of the low pressure region indicate the effects of inherent unsteadiness and the passing wakes shed from the vane trailing edge. This region of minimum pressure is an indicator of mixing out of the passage vorticities (including passage vortex, suction corner vortex) and turbulent flow with high velocity. As time passes, this low pressure region extends and contracts. In the presence of inlet skewed boundary layers (r=0.32 and 0.61), the local pressure in the fore part of the passage becomes more fluctuating, indicating the interaction between the inlet skewed boundary layers and the endwall secondary flows. Overall, the effects of inlet skewed boundary layers on the endwall pressure is negligible.

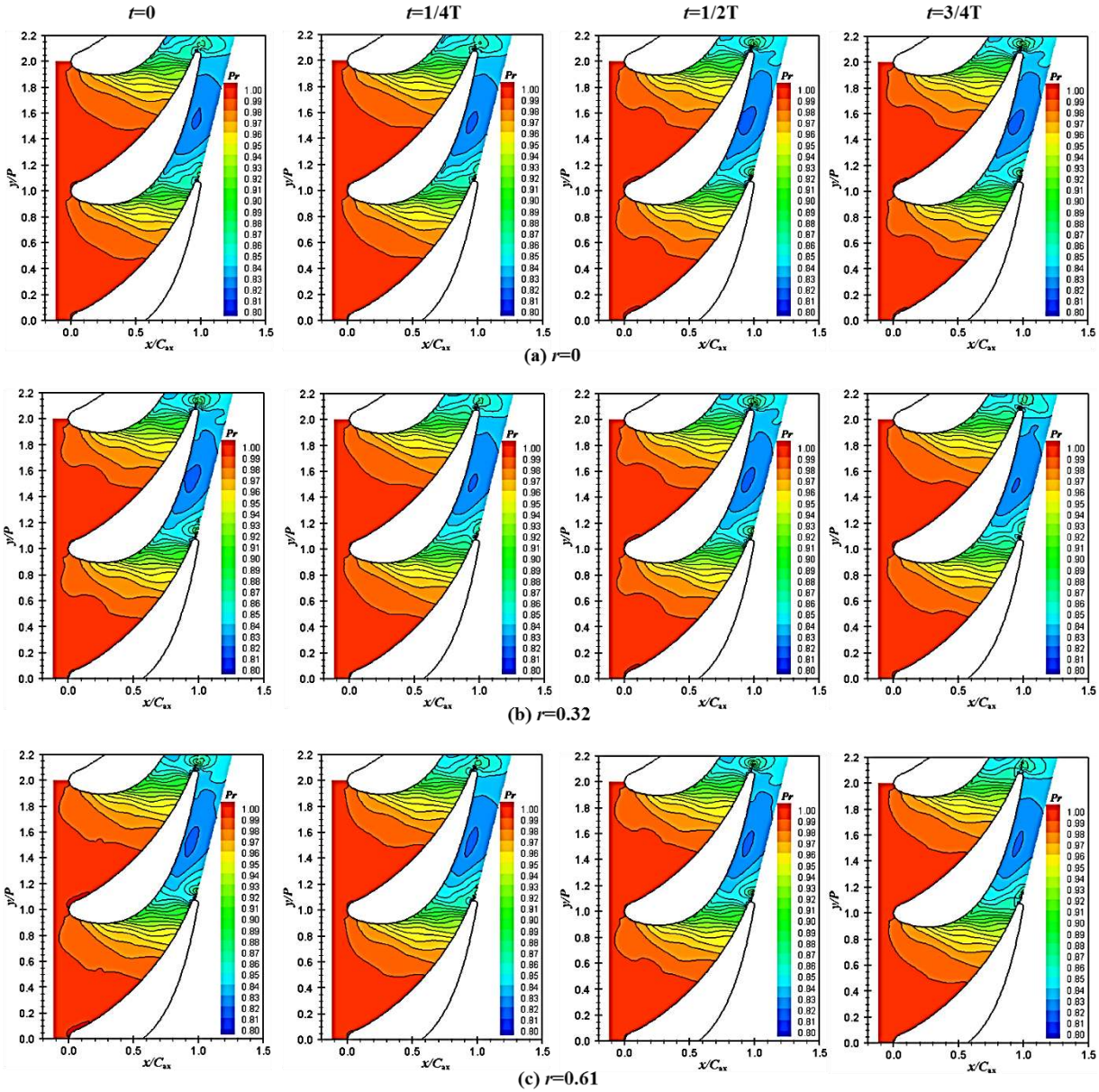

Figure 9: Instantaneous and time-averaged pressure on endwall for a flow cycle

The pressure distributions on the endwall plotted in Fig. 9 also indicates a greater pressure gradient between the pressure side and suction side of the passage. This can lead to strong cross flows from the pressure side toward the suction side within the passage. Time-averaged streamlines on the endwall are displayed in Fig. 10. The strong cross flows can be easily identified. Furthermore, the lift-off lines of the suction side leg of the horseshoe vortex and the passage vortex are visible. The inlet skew has little impact on the cross flows downstream of the passage vortex, but generates more skewed streamlines in the region upstream of the passage vortex. With the inlet skew, the suction side leg of the horseshoe vortex and the passage vortex meet the suction side of the passage in a more upstream position. This is because of the tangential (pitchwise) velocity component driven by the upstream wall moving from the pressure side to the suction side. As the upstream wall moves with a higher velocity, the pitchwise velocity component is increased, as shown in Fig. 11(b), which plots the pitchwise velocity distributions along a spanwise line at the passage inlet. Figure 11(a) shows the inlet streamwise velocity profile at the same location. There is no discernable difference between the cases of r=0 and r=0.32 but the velocity profile with r=0.61 becomes a little sharper, generating a little greater displacement thickness of boundary layer. From Figs. 11(a) and (b), one can note that the impact of the inlet skew on the flowfield only happens very close to the endwall within the boundary layer. Since the endwall secondary flows are originated from the boundary layer, it is believed that the vorticities within the passage could be affected by the inlet skew as well.

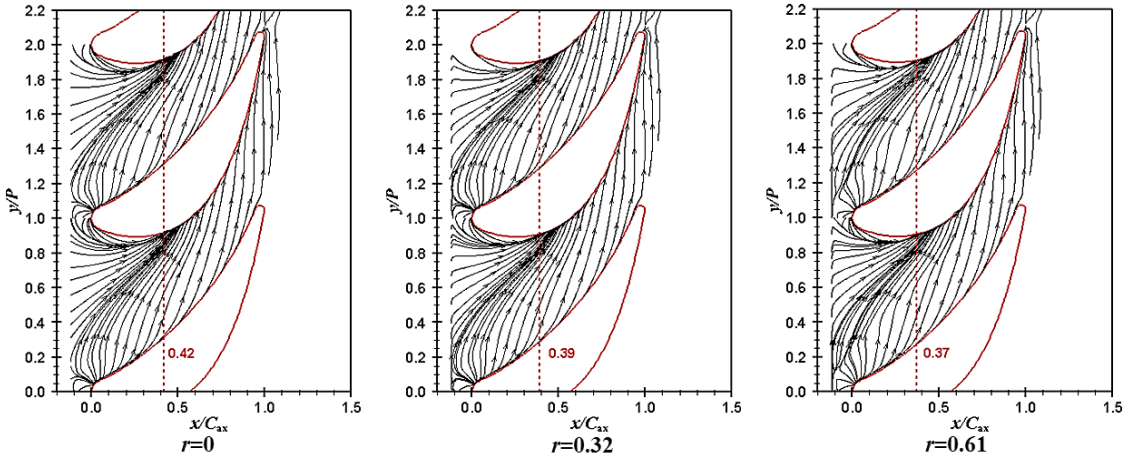

Figure 10: Time-averaged streamlines on endwall

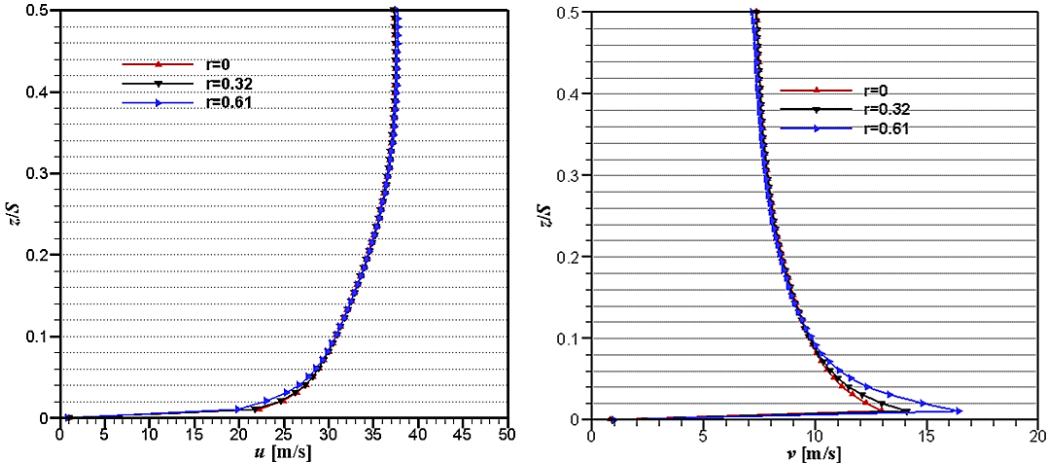

(a) Streamwise velocity component **(b) Pitchwise velocity component**

Figure 11: Time-averaged streamwise and pitchwise velocity profiles at the mid-passage of endwall passage inlet

In order to examine the effects of inlet skew on the passage vorticities, the differences in time-averaged x-axis vorticity ($\Delta\omega_x=\omega_{r=0.32\text{ or }0.61}-\omega_{r=0}$) between cases with r=0.32 and 0.61 and case with r=0 is shown in Fig. 12. The differences are made on the plane at x/C_{ax}=0.13. There are larger

differences in the local region near the suction side of the passage between cases of r=0.32 and r=0 cases, which is in accordance with the results from the streamline contours in Fig. 10. With the increase of r from 0.32 to 0.61, the region of difference in x-axis vorticity extends in the vane-to-vane direction. The difference mainly appears in the region of the suction side leg of the horseshoe vortex and the passage vortex because the inlet skew impacts the boundary layer nearby the endwall only.

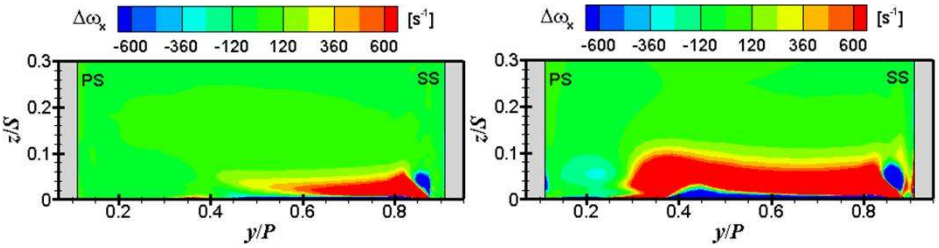

(a) Difference of x-axial vorticities between r=0.32 and r=0

(b) Difference of x-axial vorticities between r=0.61 and r=0

Figure 12: Differences in time-averaged vorticity in x direction between the stationary and moving wall cases on the plane at x/C_{ax}=0.13

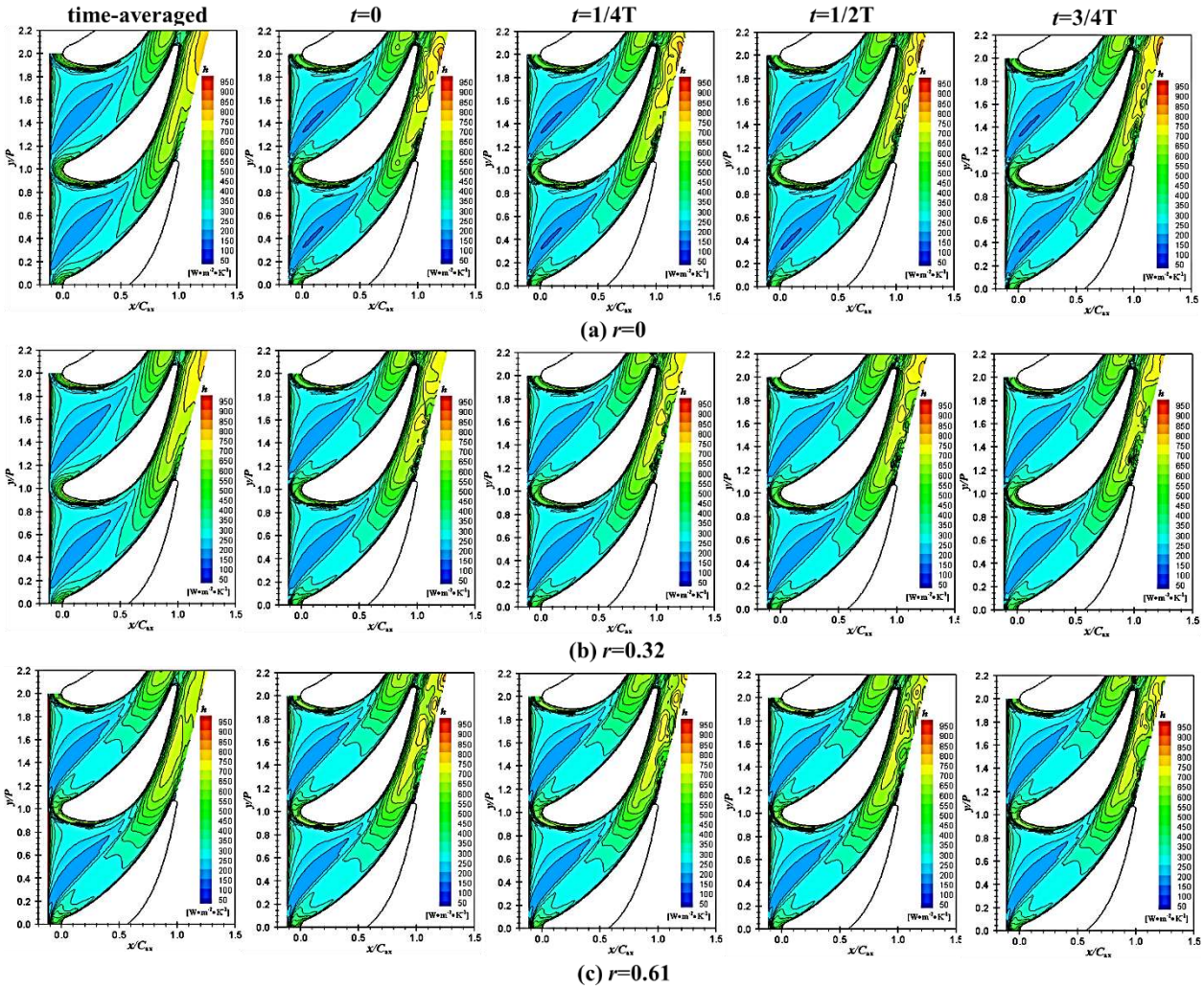

(a) r=0

(b) r=0.32

(c) r=0.61

Figure 13: Instantaneous and time-averaged heat transfer coefficient distributions on endwall for a flow cycle

The instantaneous heat transfer coefficient distributions on the endwall in Fig. 13 suggest the effects of unsteadiness and the inlet skew passage on the endwall heat transfer. In discussing the pressures of Fig. 9, we focus on the low pressure region near the suction side beyond the passage. In Fig. 13, temporal behaviors of heat transfer are also found in this region. It appears that the heat transfer characteristics have "unsteadiness" and there are significant changes in local heat transfer

levels. When the wall upstream of the endwall moves, the heat transfer in this region varies periodically, but has a slightly reduced level. This could be attributed to the sharper inlet velocity profile generated by the inlet skew (see Fig. 11(a)). In the experimental work by Choi et al. (2017), they also found that sharper inlet velocity profile generated lower overall heat transfer coefficients on the endwall. In addition to the reduced heat transfer levels by the inlet skew, the heat transfer patterns along the pressure side of the passage are changed by the inlet skew as well, especially for the case of r=0.61. The reason can be found in Fig. 12(a), in which increasing the wall velocity extends the impacts of the inlet skew toward the pressure side of the passage. The inlet skew generates variations in local heat transfer values though, the laterally-averaged heat transfer coefficients in Fig. 14 suggest that the inlet skew has little effects on the overall heat transfer over the endwall surfaces. As mentioned in the previous section, steady RANS simulations have higher predictions in heat transfer on the endwall, but they also provide evidence for the fact that the inlet skew has little effects on overall heat transfer on the endwall.

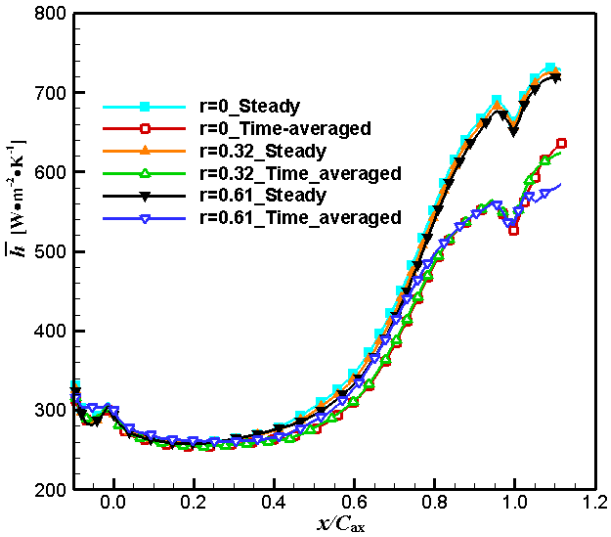

Figure 14: Laterally averaged, time-averaged heat transfer coefficients on endwall

CONCLUSIONS

Steady and unsteady RANS simulations have been performed to document the effects of inlet skewed boundary layers on endwall heat transfer due to the relative motion between blade platform and vane endwalls. Typical wall-to-axial velocity ratios of 0.32 and 0.61 are chosen to represent the actual operation of an engine. Temporal behaviors of heat transfer and pressures over the endwall surfaces have been examined in detail and the corresponding time-averaged results, compared with steady predictions, are used to evaluate the effects of unsteadiness on endwall heat transfer due to the inherent unsteadiness in flow and inlet skew passage.

Comparisons of heat transfer coefficients from steady and unsteady simulations show that the unsteadiness plays an important role in determining the endwall heat transfer. In terms of laterally-averaged heat transfer coefficient values, the time-averaged heat transfer coefficients agree fairly well with the experimental data, thereby verifying the unsteady RANS simulations of the present work. The neglect of unsteadiness using steady simulations leads to under- or over-predictions of heat transfer over most endwall surfaces. The difference in heat transfer coefficients between steady and time-averaged results in some regions is up to 20%.

The contribution of inherent unsteadiness in the flow and the inlet skew passage on the endwall pressure is negligible. The area, where the pressure is most affected by unsteadiness, is a low pressure region near the suction side beyond the passage throat. The inlet skew sweeps the flow very close to the endwall in the boundary layer toward the suction side of the passage, resulting in a little sharper inlet velocity profile and further affecting the development of the passage vortex and the suction side leg of the horseshoe vortex. This is evident from an earlier intersection of the passage vortex and horseshoe vortex with the suction surface of the vane. The inlet skew has considerable impacts on the

variation of local heat transfer coefficients and increasing the velocity ratio slightly reduces the highest heat transfer levels. However, the results both from the steady and unsteady simulations show that overall heat transfer levels on the endwall almost remain the same for all the cases.

ACKNOWLEDGMENT

The authors would like to acknowledge support from the Key Project of National Natural Science Foundation of China (Grant No. 51336007) for this work and also the Minnesota Supercomputing Institute (MSI) for providing computational resources to conduct this study.

REFERENCES

Arisi, A., Mayo, D., Li, Z., Ng, W. F., Moon, H. K., Zhang, L. Z., (2016). *An experimental and numerical investigation of the effect of combustor-nozzle platform misalignment on endwall heat transfer at transonic high turbulence conditions*. ASME Paper GT2016-57763.

Bindon, J., (1979). *Effect of hub inlet boundary layer skewing on the endwall shear flow in an annular turbine cascade*. ASME Paper No. 79-GT-13.

Bindon, J., (1980). *Exit Plane and Suction Surface Flows in an Annular Turbine Cascade with a Skewed Inlet Boundary Layer*. International Journal of Heat and Fluid Flow, 2(2), p. 57-66.

Carrick, H. B., (1977). *Secondary flow and losses in turbine cascades with inlet skew*. AGARD CP 214, Secondary Flows in Turbomachines, Paper No. 9.

Celik, I. B., Ghia, U., Roache, P. J., Freitas, C. J., Coleman, H., and Raad, P. E., (2008). *Procedure for estimation and reporting of uncertainty due to discretization in CFD applications*. Journal of Fluids Engineering, 130, p. 078001.

Choi, S. M., Kim, J., Bang, M., Kim, J. J., and Cho, H. H., (2018). *Effect of the Wake on the Heat Transfer of a Turbine Blade Endwall According to Relative Position of the Cylindrical Rod.* International Communications in Heat and Mass Transfer, 94, pp. 61-70.

Choi, S. M., Park, J. S., Chung, H., Park, S., and Cho, H. H., (2017). *Upstream wake effect on flow and heat transfer characteristics at an endwall of first-stage blade of a gas turbine*, Experimental Thermal Fluid Science, 86(2017), pp. 23-36.

Dullenkopf, K., Schulz, A., and Wittig, S., (1991). *The effect of incident wake conditions on the mean heat transfer of an airfoil*. Journal of Turbomachinery, 113(3), p. 412-418.

El-Gabry, L. A., Ameri, A. A., (2011). *Comparison of steady and unsteady rans heat transfer simulations of hub and endwall of a turbine blade passage*. Journal of Turbomachinery, 133, p. 031010.

Ghosh, K. and Goldstein, R. J., (2012). *Effect of inlet skew on heat/mass transfer from a simulated turbine blade*. Journal of Turbomachinery, 134, p. 051042.

Giel, P. W., Thurman, D. R., Fossen, G. J. V., Hippensteele, S. A., and Boyle, R. J., (1998). *Endwall heat transfer measurements in a transonic turbine cascade*. Journal of Turbomachinery, 120(2), pp. 305-313.

Graziani, R. A.., Blair, M. F., Taylor, R. J., and Mayle, R. E., (1980). *An experimental study of endwall and airfoil surface heat transfer in a large scale turbine blade cascade*. Journal of Engineering for Gas Turbines and Power, 102(2), pp. 602-602.

Harvey, N. W., Rose, M. G., Coupland, J., and Jones, T. V., (1999). *Measurement and calculation of nozzle guide vane end wall heat transfer*. Journal of Turbomachinery, 121(2), pp. 184-190.

Kang, M. B., Kohli, A., and Thole, K. A., (1999). *Heat transfer and flowfield measurements in the leading edge region of a stator vane endwall*. Journal of Turbomachinery, 121(3), p. 558-568.

Laveau, B., Abhari, R. S., Crawford, M. E., et al. (2014). *High resolution heat transfer measurements on the stator endwall of an axial turbine*. Journal of Turbomachinery, 137(4), p. 041005.

Lutum, E., Cottier, F., Crawford, M. E., et al. (2015). *A computational investigation of the effect of surface roughness on heat transfer on the stator endwall of an axial turbine*. Journal of Power and Energy, 229(5), pp. 2165-2168.

Papa, M., Goldstein, R. J., and Gori, F., (2007). *Numerical heat transfer predictions and mass/heat transfer measurements in a linear turbine cascade*. Applied Thermal Engineering, 27 (4), pp. 771-778.

Pasinato, H. D., Squires, K. D., Roy, R. P., (2004), *Assessment of Reynolds-averaged turbulence models for prediction of the flow and heat transfer in an inlet vane-endwall passage*. Journal of Fluids Engineering, 126(3), pp. 305-315.

Radomsky, R. W. and Thole, K. A., (2000). *High free-steam turbulence effects on endwall heat transfer for a gas turbine stator vane*. Journal of Turbomachinery, 122(4), pp. 699-708.

Schobeiri, M., Ozturk, B., and Ashpis, D., (2005). *On the physics of flow separation along a low pressure turbine blade under unsteady flow conditions*. Journal of Fluids Engineering, 127(3), p. 503-513.

Schobeiri, M., Ozturk, B., and Ashpis, D., (2007). *Effect of Reynolds number and periodic unsteady wake flow condition on boundary layer development, separation, and intermittency behavior along the suction surface of a low pressure turbine blade*. Journal of Turbomachinery, 129(1), p. 92-197.

Simon, T. W., and Piggush, J. D., (2006). *Turbine endwall aerodynamics and heat transfer*. Journal of Propulsion and Power, 22(2), pp. 301-312.

Walsh, J. and Gregory-Smith, D., (1987). *Effect of inlet skew on the secondary flows and losses in a turbine cascade*. Proceedings of Institute of Mechanical Engineers, International Conference "Turbomachinery–Efficiency Prediction and Improvement", Paper No. C275/87.

Walsh, J. and Gregory-Smith, D., (1990). *Inlet skew and the growth of secondary losses and vorticity in a turbine cascade*. Journal of Turbomachinery, 112(4), p. 633-642.

Wang, H., Olson, S., Goldstein, R., and Eckert, E., (1997). *Flow visualization in a linear turbine cascade of high performance turbine blades*. Journal of Turbomachinery, 119(1), pp. 1-8.

Yang, X., Liu, Z. S., Zhao, Q., Liu, Z., Feng, Z. P., Guo, F. S., and Ding, L., (2017). *Experimental investigations and numerical analysis on heat transfer of a ngv endwall at engine representative Reynolds and Mach Numbers*. Proceedings of Shanghai 2017 Global Power and Propulsion Forum, GPPS-2017-0128.

Zhang, L., and Han, J. C., (1995). *Combined effect of free-stream turbulence and unsteady wake on heat transfer coefficients from a gas turbine blade*. Journal of Heat Transfer, 117(2), p. 296-302.